Braz J Phys (2014) 44:128–137
DOI 10.1007/s13538-013-0171-9

SOCIEDADE BRASILEIRA DE FÍSICA

PARTICLES AND FIELDS

Black Hole Scattering via Spectral Methods

P. C. M. Clemente · H. P. de Oliveira · E. L. Rodrigues

Received: 23 July 2013 / Published online: 15 December 2013

Abstract We present an alternative method to solve the problem of scattering by a black hole by adapting the spectral code originally developed by Boyd (*Comp Phys* 4:83, 1990). In order to show the effectiveness and versatility of the algorithm, we solve the scattering by Schwarzschild, standard acoustic, and charged black holes. We recover the partial and total absorption cross sections and, in the case of charged black holes, the conversion factor of eletromagnetic and gravitational waves. We also study the exponential decay of the reflection coefficient, which is a general feature of any scattering problem.

Keywords Spectral methods · Black hole scattering

1 Introduction

A particularly useful way of understanding the physics of a black hole spacetime is considering it as a scatterer of waves impinge on it. Black hole scattering has been studied intensively in over the last 40 years, whose prototype model is a packet of massless scalar waves hitting a Schwarzschild black hole. In general, electromagnetic and gravitational waves can be also be used to probe the spacetime around not only the Schwarzschild, but any black hole.

Perturbation theory provides the mathematical formulation of the scattering by a black hole. In order to fix the notation, let us consider, for the sake of simplicity, a scalar field Φ evolving in the Schwarzschild spacetime. It can be shown that the solution of the Klein–Gordon equation $g^{\mu\nu}\Phi_{,\mu;\nu} = 0$ is expressed as a partial wave sum [2, 3],

$$\Phi(t, r, \theta) = \sum_{l=0}^{\infty} (2l+1) \mathrm{e}^{-i\omega t} \frac{\varphi_l(r)}{r} P_l(\cos\theta), \tag{1}$$

for which the functions $\varphi_l(r)$ satisfy a Schrodinger-like equation,

$$\frac{d^2\varphi_l}{dx_*^2} + \left(\omega^2 - V_{\mathrm{eff}}(x)\right)\varphi_l = 0, \tag{2}$$

where $x = r/2M \geq 1$, $x_* = r_*/2M \in (-\infty, +\infty)$, M is the black hole mass, and r_* is the tortoise coordinate defined by $dr_*/dr = r/(r-2M)$. Also, $V_{\mathrm{eff}}(x) = 4M^2V(r(x))$ is the effective potential induced by the black hole spacetime, and due to the rescaling of the radial coordinate, we are adopting $\omega \to 2M\omega$.

Similar Schrodinger-like equations describe the scattering of electromagnetic and gravitational waves, in which the form of the effective potential [4] is modified in each case. Important physical issues can be studied from Eq. (2): the stability problem of the Schwarzschild black holes [5], the determination of the black hole response to perturbations through their quasi-normal modes [6] of vibration, and the black hole scattering problem in which the amount of scattered and transmitted waves can be evaluated as well as the absorption cross sections [2–4, 7].

In order to solve the scattering problem, one can apply the perturbation theory or the partial wave method. The perturbation theory is more appropriate in the long-wavelength limit, and the partial wave method [2, 3] is more suitable beyond the long-wavelength regime. Essentially, it consists of solving the corresponding Schrodinger equation at the

P. C. M. Clemente · H. P. de Oliveira (✉) · E. L. Rodrigues
Departamento de Física Teórica, Instituto de Física, Universidade do Estado do Rio de Janeiro, Rua São Francisco Xavier, 524, 20550-013 Rio de Janeiro, Brazil
e-mail: hahuga@gmail.com

horizon and at the asymptotically flat region characterized by assuming it at some $r = r_{\max}$. The scattered wave is calculated after discarding the part of the solution corresponding to the original plane wave, whose definition in curved spacetimes is done by an analogy with the Coulomb scattering. We mention also the approach using the phase integral method applied to the problem of scattering of massless waves by a Schwarzschild black hole [8].

Boyd [1] devised a pseudospectral algorithm to solve the problem of wave scattering by a potential barrier in a typical one-dimensional quantum mechanical problem. He introduced the special radiation functions to overcome the fact that any basis sets cannot model the incoming and the outgoing waves. In his pioneering work, he solved the problem of wave scattering by a sech^2 potential barrier with success. In this way, it is worth investigating the applicability of this method to the black hole scattering problem. To achieve this goal, we have implemented some modifications of the original Boyd's procedure to adapt it to the case of the scattering by a black hole and also to improve its accuracy.

The structure of the paper is as follows: in Section 2, we present Boyd's spectral algorithm to the black hole scattering problem and introduce some modifications that improve the accuracy of the algorithm. In Section 3, we apply the method to the Schwarzschild and the standard acoustic black holes. We evaluate the transmission and reflection coefficients as well as the relevant quantities such the partial and total absorption cross sections. We have considered the scattering by Reissner–Nordström black holes in Section 4. In particular, we have focused in determining the conversion factor of electromagnetic to gravitational perturbations and vice versa. Finally, in Section 5 we present our conclusions.

2 Boyd's Method Revisited

We present the procedure envisaged by Boyd [1] to tackle the problem of wave scattering described by Eq. (2). As a typical problem of wave scattering, we consider ω to be real which produces solutions representing ingoing and outgoing waves at the boundaries of the spacetime, $x_* \to \pm\infty$. In this vein, we establish the following boundary conditions, recalling that the effective potential vanishes at the boundaries:

$$\varphi = \begin{cases} \mathrm{e}^{-i\omega x_*} + \alpha(\omega)\mathrm{e}^{i\omega x_*} & x_* \to \infty \\ \\ \beta(\omega)\mathrm{e}^{-i\omega x_*}, & x_* \to -\infty. \end{cases} \tag{3}$$

These conditions represent an incident wave of unit amplitude, a reflected wave with amplitude $\alpha(\omega)$, both at the spatial infinity ($x_* \to \infty$), and a transmitted wave of amplitude $\beta(\omega)$ crossing the event horizon ($x_* \to -\infty$). From these amplitudes, one can calculate the reflection and transmission coefficients: $R(\omega) = |\alpha(\omega)|^2$ and $T(\omega) = |\beta(\omega)|^2$, respectively. They are subjected to the condition

$$R(\omega) + T(\omega) = 1, \tag{4}$$

which insures energy conservation in the scattering problem described by Eq. (2). In other words, it expresses the fact that an incident wave of unitary amplitude after hitting a potential barrier splits into two pieces of reflected and transmitted waves whose sum of the square of their amplitudes is 1 [4].

In order to determine $R(\omega)$ and $T(\omega)$ using spectral methods, Boyd introduced the special radiation functions since standard Chebyshev polynomials are unable to reproduce the asymptotic oscillatory behavior given by Eq. (3).

Consider the real-valued functions $C(x_*)$ and $S(x_*)$ whose asymptotic behavior is

$$C(x_*) \sim \cos(\omega x_*), \;\; S(x_*) \sim \sin(\omega x_*), \;\; \text{as} \;\; x_* \to \infty. \tag{5}$$

Notice that these solutions are the linearly independent solutions of Eq. (2) at $x_* \to \infty$, implying that its general solution can be expressed as a linear combination of $C(x_*)$ and $S(x_*)$. Then, taking into account the boundary conditions at the spatial infinity, we obtain

$$\varphi = (1+\alpha)C(x_*) + i(\alpha - 1)S(x_*). \tag{6}$$

The next step is to establish the asymptotic behavior of the functions $C(x_*)$ and $S(x_*)$ near the event horizon, $x_* \to -\infty$,

$$C(x_*) \;\; \sim \gamma_1 \cos(\omega x_*) + \gamma_2 \sin(\omega x_*), \tag{7}$$

$$S(x_*) \;\; \sim \bar{\gamma}_1 \cos(\omega x_*) + \bar{\gamma}_2 \sin(\omega x_*). \tag{8}$$

Substituting Eqs. (7) and (8) into Eq. (6), we obtain the behavior of φ at the event horizon. If we combine this result with the boundary condition given by Eq. (3), it follows that

$$\begin{cases} (1+\alpha)\gamma_1 + i(\alpha-1)\bar{\gamma}_1 = \beta \\ \\ (1+\alpha)\gamma_2 + i(\alpha-1)\bar{\gamma}_2 = -i\beta. \end{cases} \tag{9}$$

This system can be solved to determine the real and imaginary parts of (α, β) once the coefficients $(\gamma_1, \gamma_2, \bar{\gamma}_1, \bar{\gamma}_2)$ become known using the collocation method as we are going to describe.

Following Boyd [1], the functions $C(x_*)$ and $S(x_*)$ must contain plane wave components to describe asymptotically oscillatory behavior present in Eqs. (5), (7), and (8). Then,

$$C(x_*) = \cos(\omega x_*) + \bar{C}(x_*) \tag{10}$$

$$S(x_*) = \sin(\omega x_*) + \bar{S}(x_*), \tag{11}$$

where the auxiliary functions $\bar{C}(x_*)$, $\bar{S}(x_*)$ approach zero as $x_* \to \infty$. The spectral representation of these functions is

$$\bar{C}(x_*) = \sum_{k=0}^{N-2} a_k \chi_k(x_*) + a_{N-1}\phi_C(x_*) + a_N \phi_S(x_*) \quad (12)$$

$$\bar{S}(x_*) = \sum_{k=0}^{N-2} b_k \chi_k(x_*) + b_{N-1}\phi_C(x_*) + b_N \phi_S(x_*), \quad (13)$$

where (a_k, b_j) are the modes and $\phi_C(x_*)$ and $\phi_S(x_*)$ are the radiation functions [1] for which

$$\phi_C(x_*), \phi_S(x_*) \to 0, \text{ as } x_* \to \infty. \quad (14)$$

On the other hand, when $x_* \to -\infty$, the asymptotic behavior described by Eqs. (7) and (8) must be reproduced. In this case, we have

$$\phi_C(x_*), \phi_S(x_*) \to \cos(\omega x_*), \sin(\omega x_*), \text{ as } x_* \to -\infty. \quad (15)$$

Boyd [1] assumed that the radiation functions reproduce the boundary conditions (14) and (15),

$$\phi_C(x_*) = \frac{1}{2}[1 - \tanh(\epsilon_0 x_*)]\cos(\omega x_*) \quad (16)$$

$$\phi_S(x_*) = \frac{1}{2}[1 - \tanh(\epsilon_0 x_*)]\sin(\omega x_*), \quad (17)$$

where the coefficient ϵ_0 was introduced so that $\phi_{C,S}$ vary on the same scale as V_{eff} [9]. This parameter was not present in the original Boyd's algorithm.

At this point, we have introduced another modification in the original Boyd's scheme. Instead of choosing the rational Chebyshev functions, $TB_k(x_*)$ [10], we have selected the basis $\chi_k(x_*)$ defined by

$$\chi_k(x_*) \equiv \frac{1}{2}(TB_{k+2}(x_*) - TB_k(x_*)) \quad (18)$$

that satisfies exactly the condition $\chi_k(x_*) \to 0$ as $x_* \to \pm\infty$. As noted first by Heinrichs [11–13], a recombination of the usual pure Chebyshev basis functions produces more accurate results due to lower accumulated round off error when solving higher-order differential equations.

With the above conditions, it follows that $C(x_*) = \cos(\omega x_*)$, $S(x_*) = \sin(\omega x_*)$ as $x_* \to \infty$, and

$$C(x_*) = (1 + a_{N-1})\cos(\omega x_*) + a_N \sin(\omega x_*) \quad (19)$$

$$S(x_*) = b_{N-1}\cos(\omega x_*) + (1 + b_N)\sin(\omega x_*), \quad (20)$$

as $x_* \to -\infty$, which provides that $\gamma_1 = 1 + a_{N-1}$, $\gamma_2 = a_N$, $\bar{\gamma}_1 = b_{N-1}$, and $\bar{\gamma}_2 = 1 + b_N$. Thus, once the modes (a_k, b_j) are determined, the coefficients of Eqs. (7) and (8) become known, and we can solve the system (9) for α, β.

The next step is to substitute Eqs. (10) and (11) into Eq. (6), in which the functions $\bar{C}(x_*)$ and $\bar{S}(x_*)$ are approximated by their corresponding spectral representations given by Eqs. (12) and (13), respectively. Then, from the Schrodinger-like equation (2), we obtain two residual equations:

$$\text{Res}_C(x_*) = \frac{d^2\bar{C}}{dx_*^2} + \left[\omega^2 - V_{\text{eff}}(x)\right]\bar{C} - V_{\text{eff}}(x)\cos(\omega x_*) \quad (21)$$

$$\text{Res}_S(x_*) = \frac{d^2\bar{S}}{dx_*^2} + [\omega^2 - V_{\text{eff}}(x)]\bar{S} - V_{\text{eff}}(x)\sin(\omega x_*). \quad (22)$$

These relations do not vanish due to the approximation expressed by a finite N in the spectral representations of $\bar{C}(x_*)$ and $\bar{S}(x_*)$. In order to determine the coefficients a_k and b_j, we have considered the collocation method that consists in fixing these coefficients such that the above residual equations vanish at the collocation or grid points y_k given by

$$y_k = \cos\left[\frac{(2k+1)\pi}{2N+2}\right], \; k = 0, 1, ..., N, \quad (23)$$

where the new variable $y \in (-1, 1)$ is related to x_* through

$$x_* = x_*^{(0)} + \frac{L_0 y}{\sqrt{1 - y^2}}, \quad (24)$$

where $x_*^{(0)}$ adjusts the position of the origin of the computational domain y, L_0 is the map parameter to be chosen according to the typical scale of the potential, and $\epsilon_0 \propto 1/L_0$. We have chosen $x_*^{(0)} = x_*^{\max}$, where $x_*^{\max}$ indicates the maximum of the effective potential. We fix L_0 and ω and, therefore, the modes (a_k, b_j) can be obtained after solving linear algebraic system arising from the vanishing residual equations at the collocation points, or

$$\text{Res}_C(x_*(y_k)) = 0, \quad \text{Res}_S(x_*(y_k)) = 0, \; k = 0, 1, ..., N. \quad (25)$$

In the next section, we present the application of this scheme for several black hole spacetimes.

3 Schwarzschild and Acoustic Black Holes

The effective potential for the Schwarzschild black hole is given by [5]

$$V_{\text{eff}} = \left(1 - \frac{1}{x}\right)\left[\frac{l(l+1)}{x^2} + \frac{1-s^2}{x^3}\right], \tag{26}$$

where $s = 0, 1, 2$ denotes scalar, electromagnetic, and gravitational perturbations. The relation between x and x_* is $x_* = x + \ln(x-1)$.

There are two types of gravitational perturbations ($s = 2$): the axial (odd parity) and polar (even parity) perturbations. The corresponding effective potentials, which we denote by $V_{\text{eff}}^{(-)}(x)$ and $V_{\text{eff}}^{(+)}(x)$, respectively, are distinct. We obtain the expression for $V_{\text{eff}}^{(-)}(x)$ by setting $s = 2$ in Eq. (26). The effective potential $V_{\text{eff}}^{(+)}(x)$ is expressed as

$$V_{\text{eff}}^{(+)} = \frac{8}{(2nx+3)^2}\left(1 - \frac{1}{x}\right)\left[n^2(n+1) + \frac{3n^2}{2x} + \frac{9n}{4x^2} + \frac{9}{8x^3}\right], \tag{27}$$

where $2n = (l-1)(l+2)$. In spite of both potentials being distinct, Chandrasekhar [4] demonstrated a remarkable relation between the solutions of the Schrodinger equation for both types of perturbations. As a consequence, the reflection and transmission coefficients are the same no matter if the gravitational perturbations are axial or polar.

Applying the numerical scheme presented in the previous section, we have solved the scattering problem by determining the real and imaginary parts of α and β in function of ω for fixed values of l and s. We have checked the accuracy of the code using the transmission and reflection coefficients, $T(\omega) = |\beta|^2$ and $R(\omega) = |\alpha|^2$, respectively, to calculate the deviation of Eq. (4) taken as the basic measure of the error

$$\delta = |R(\omega) + T(\omega) - 1| \times 100. \tag{28}$$

The first task is to confirm whether or not the new basis function, $\chi_k(x_*)$, produces more accurate results than the pure rational Chebyshev basis function, $TB_k(x_*)$. We have calculated the error for gravitational perturbations $s = 2$ and $l = 4$, taking a region where R is very small. According to Fig. 1, the improvement of the accuracy becomes clear due to the overall smallness of the error when evaluated using the new basis functions. This result is also valid for any other choice of the parameters. Hereafter, unless stated otherwise in all figures, we represent the numerical results by solid circles and join them by lines for the sake of convenience.

Another numerical test is to verify if the reflection and transmission coefficients for polar and axial perturbations,

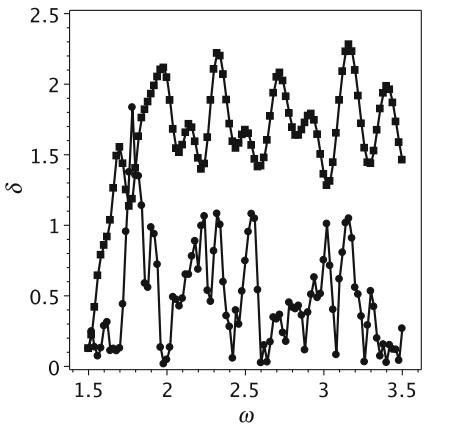

Fig. 1 Error δ for the case $l = 4$ and $s = 2$ (gravitational perturbations) with truncation order $N = 80$. The curves formed with *solid boxes* and *circles* correspond to the numerical results obtained using the basis $TB_k(x_*)$ and $\chi_k(x_*)$, respectively. The improvement due to the new basis functions becomes clear where for some values of ω, the error becomes an order of magnitude smaller

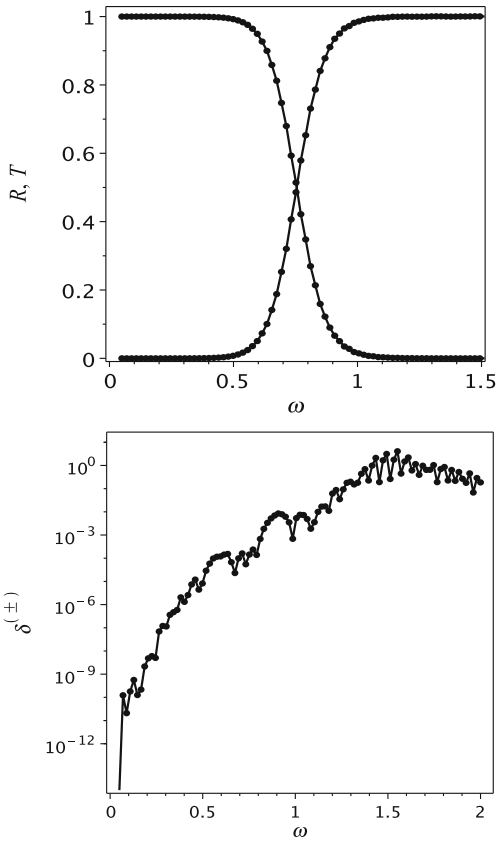

Fig. 2 Typical behavior of the reflection ($R \sim 1$ for small frequencies) and transmission coefficients. In the first plot, the *continuous lines* and *dots* were determined using the effective potentials $V_{\text{eff}}^{(-)}$ and $V_{\text{eff}}^{(+)}$, respectively. The agreement of these coefficients evaluated is clear, but in the second plot, we have displayed the error $\delta^{(\pm)}$ quantifying the deviation of both values of $R(\omega)$. We have selected $N = 300$, $L_0 = 14$, and $\epsilon_0 = 2/L_0$

$R^{(+)}(\omega)$ and $R^{(-)}(\omega)$, respectively, are equal. In Fig. 2a, we present a typical plot of both $R^{(-)}, T^{(-)}$ (lines) and $R^{(+)}, T^{(+)}$ (dots). In order to quantify the deviation of equality between both coefficients, we use $\delta^{(\pm)} \equiv |R^{(+)} - R^{(-)}|/R^{(-)} \times 100$, whose graph is shown in Fig. 2b. We have repeated this verification for different values of l and found that both coefficients coincide within an acceptable error.

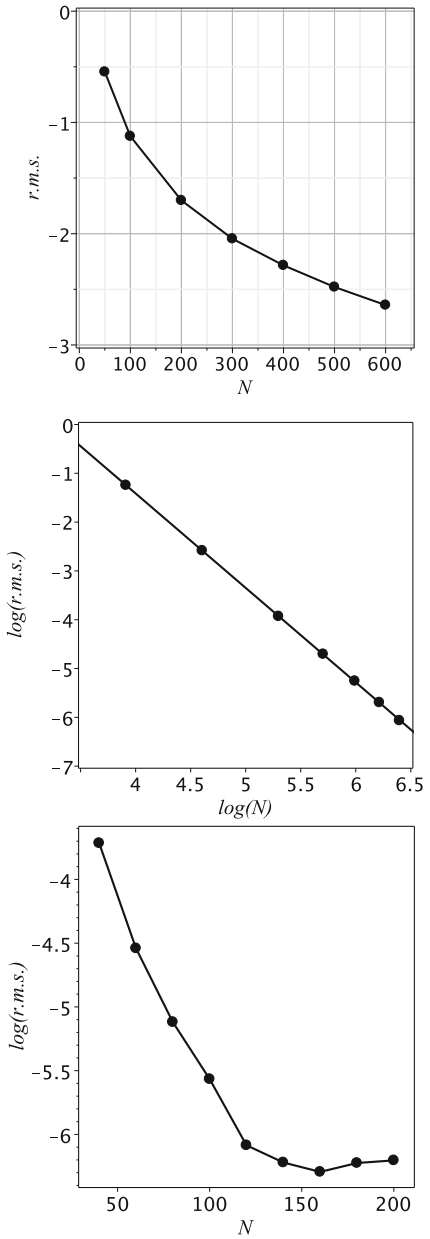

Fig. 3 Plot of small $R(\omega)$ for $l = 2$ and $s = 1$ (vectorial perturbations) with truncation orders $N = 50, 100, 600$. In the *second panel*, we show the decay of the error rms given by $\left(1/M \sum_{k=1}^{M} \delta_i^2\right)^{1/2}$. We have found that the error decays as $N^{-1.93}$. In a region in which $R \approx 1$, the decay is exponential as shown in the *third graph*

In all numerical experiments, we have noticed an increase of the error in determining the small values of the reflection coefficient. This is a consequence of the exponential decay of $R(\omega)$, which is a general feature of any scattering problem as pointed out by Boyd [1]. To overcome this difficulty, the Schrodinger equation must be solved to very high accuracy for a reasonable approximation to $R(\omega)$ for large ω. We present a convergence test by displaying in Fig. 3 the behavior of $R(\omega) \ll 1$, taking increasing truncation orders and the decay of the errors. However, we point out that small truncation orders are adequate to solve the scattering problem when $R(\omega) \sim 1$.

Usually, in problems of wave scattering, the absorption cross section is another quantity that depends only on the asymptotic behavior of the waves. The absorption cross section is given by [15],

$$\sigma_{\text{abs}} = \sum_{l=l_{\text{min}}}^{\infty} \sigma_{\text{abs}}^{(l)}, \tag{29}$$

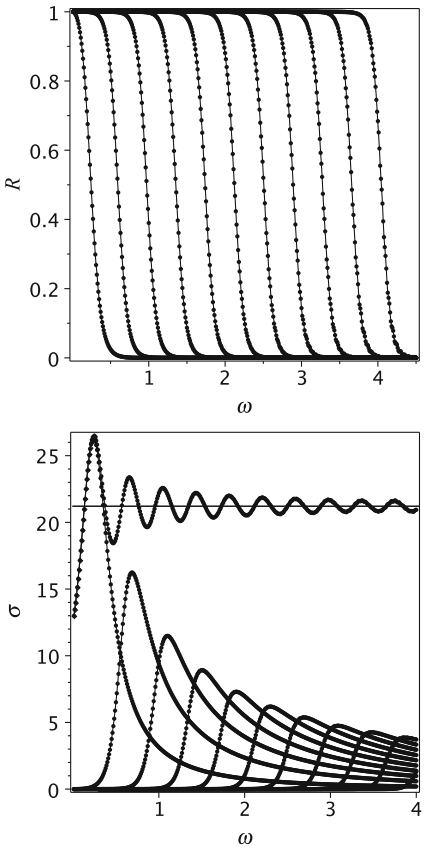

Fig. 4 Reflection coefficients $R_l(\omega)$ for scalar perturbations. From *left* to *right*: the curves correspond to the cases $l = 0, 1, 2, ..., 10$. *Second plot*: the partial and total absorption cross sections in units of M^2. The total absorption cross section tends to the analytical result of geometrical optics indicated by the *straight line*

where $l_{\min} = 0, 1, 2$ for scalar, electromagnetic, and gravitational perturbations. The partial absorption cross section, $\sigma_{\text{abs}}^{(l)}$, is related to the transmission coefficient $T(\omega)$ through

$$\sigma_{\text{abs}}^{(l)} = \frac{\pi}{\omega^2}(2l+1)T_l(\omega). \tag{30}$$

In Fig. 4, we present the reflection coefficients $R(\omega)$ for $l = 0, 1, ..., 10$ for scalar perturbations ($s = 0$). The truncation orders vary from $N_{\min} = 100$ to $N_{\max} = 500$ depending on the chosen value of l, such that the error δ never exceeds 0.2 % to produce smooth curves. With these data, we show in the second graph of Fig. 4 the partial and total absorption cross sections for the scalar perturbations. The total absorption cross section tends to the predicted geometric optics value [16] given by $\sigma_{\text{abs}} = 27\pi M^2/4 \approx 21.21M^2$ (the factor 1/4 comes from our rescaling $\omega \to 2M\omega$). We also have solved the scattering problem for gravitational perturbations ($s = 2$) for $l = 2, 3, ..., 9$ and present in Fig. 5 the plots of the partial and total absorption cross sections. In this case, the numerical result tends to the predicted value of the total absorption cross section in the high-frequency limit, which is the same of the scalar perturbations.

The canonical acoustic hole [17, 18] is the simplest analogue black hole which may be created in a laboratory. In this analogue, no sound waves can escape from a given region limited by a horizon. It can be shown that, as a response of fluid perturbations, the canonical acoustic hole produces the following effective potential:

$$V_{\text{eff}} = \left(1 - \frac{1}{x^4}\right)\left[\frac{l(l+1)}{x^2} + \frac{4}{x^6}\right], \tag{31}$$

where $x = r/r_c$ with r_c as the distance from the origin to the point at which the flow speed exceeds the sound velocity in the fluid. As a consequence, it follows that in the Schrodinger equation (2), $\omega \to \omega r_c$. The relation between x and x_* is obtained from $dx_*/dx = x^4/(x^4 - 1)$.

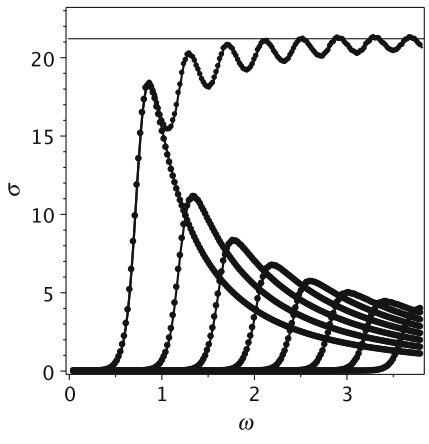

Fig. 5 Partial and total absorption cross sections in units of M^2 for gravitational perturbations for $l = 2, 3, ..., 9$. The total absorption cross section tends to the same geometrical optics limit $\sigma_{\text{abs}} = 21.21M^2$ as expected

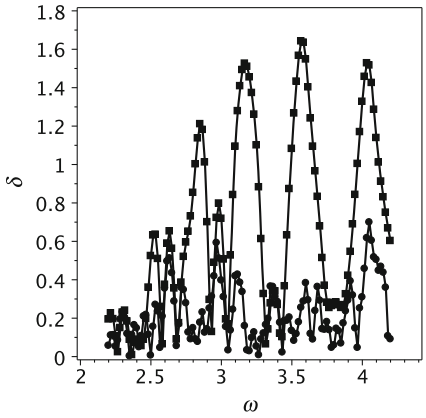

Fig. 6 Error δ for the case $l = 4$ with truncation order $N = 100$. The *upper graph* (*solid boxes*) corresponds to the basis $TB_k(x_*)$, and the *lower graph* (*solid circles*) the basis and $\chi_k(x_*)$. The improvement due to the new basis functions is clear where for some values of ω, the error becomes an order of magnitude smaller

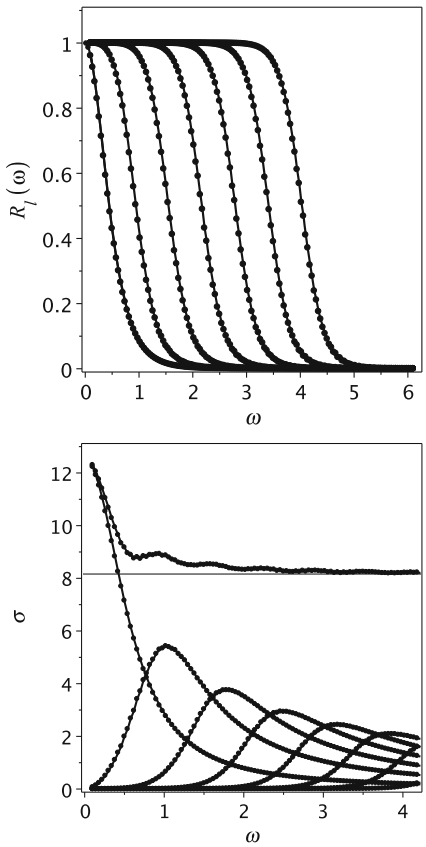

Fig. 7 Reflection coefficients for $l = 0, 1, ..., 7$ (from *left* to *right*). The truncation orders vary from a minimum value of $N = 150$ to a maximum of $N = 450$ for $l = 0$ and 7, respectively. In all cases, $L_0 = 14$. The partial and total absorption cross sections are shown in the *second panel*. Notice that the limit value of the total absorption cross section for high frequencies is in agreement with its geometric optics value $\sigma_{\text{abs}} \simeq 8.163r_c^2$ [19]

The error δ is evaluated for the case of acoustic hole and considering the basis functions $\chi_k(x_*)$ and $TB_k(x_*)$. The result shown in Fig. 6 confirmed that the first basis functions are preferable than the pure Chebyshev polynomials.

We have solved the scattering problem for $l = 0, 1, ..., 7$ and plotted the corresponding reflection coefficients in Fig. 7. Its behavior is in agreement with the results of Dolan et al. [19]. The partial and total absorption cross sections are also computed and depicted in Fig. 7. The numerical value of the total absorption cross section for high frequencies is in agreement with the geometric optics limit $\sigma_{\text{abs}} \simeq 8.163 r_c^2$ [19].

We now examine the exponential decay of the reflection coefficient described by $R(\omega) \sim \exp(-\kappa\omega)$, which is a general feature of any scattering problem. We have determined the coefficient κ for the scattering by Schwarzschild and standard acoustic black holes (Fig. 8). In both cases, the numerical experiments have indicated that κ tends to a constant value for large l. In particular, for the scattering by Schwarzschild, this limit value is independent of the type of perturbations ($s = 0, 1, 2$). Although not shown here, the same results are valid for the scattering by a charged black hole, which we consider in the next section.

4 Reissner–Nordström Black Holes

The problem of wave scattering by charged black holes can be divided into two parts. The first part deals with the problem of scalar waves, whose treatment is similar to the previous cases but with a different effective potential. The second part deals with the scattering of electromagnetic and gravitational waves. These two forms of perturbations couple via charge; for this reason, they cannot be treated independently. It means that if a purely gravitational radiation is incident on a charged black hole, a given amount is reflected as electromagnetic waves and conversely. This is the simplest scenario in which the relativistic phenomenon of conversion of gravitational energy into electromagnetic energy and vice versa [4, 20] takes place. Therefore, after determining the transmission and reflection coefficients associated to electromagnetic and gravitational waves, the conversion factor between these forms of radiation can be evaluated.

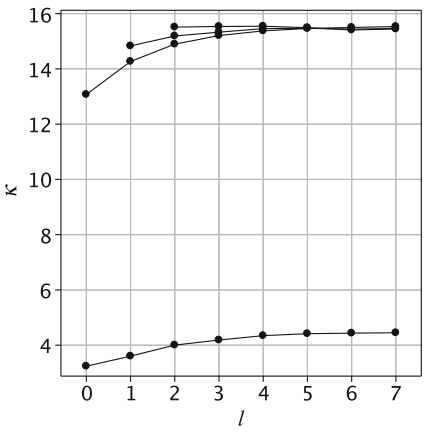

Fig. 8 Behavior of κ for the scattering of scalar ($l \geq 0$), vectorial ($l \geq 1$), and tensorial ($l \geq 2$) perturbations by a Schwarzschild black hole. The *lower plot* represents the case of scattering by an acoustic hole

4.1 Scalar Perturbations

We begin with scalar perturbations. In this case, the effective potential is given by [4]

$$V_{\text{eff}}(x) = f(x)\left[\frac{l(l+1)}{x^2} + \frac{1}{x^3} - \frac{q^2}{2x^4}\right], \tag{32}$$

where $q \equiv Q/M$, M and Q are the mass and the charge of the black hole, respectively, and

$$f(x) = \left(1 - \frac{1}{x} + \frac{q^2}{4x^2}\right). \tag{33}$$

In our analysis, we are going to consider the case $0 < q < 1$ and the extremal charged black hole $q = 1$. The relation between x and x_* becomes

$$\frac{dx_*}{dx} = \frac{1}{f(x)} = \begin{cases} \frac{x^2}{(x-x_+)(x-x_-)}, & 0 \leq q < 1 \\ \frac{x^2}{\left(x-\frac{1}{2}\right)^2}, & q = 1, \end{cases} \tag{34}$$

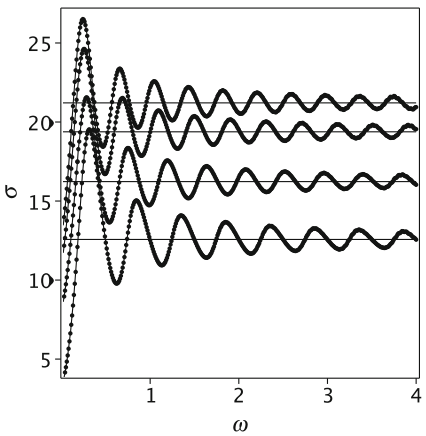

Fig. 9 Reissner–Nordström total absorption cross sections for $q = 0, 0.5, 0.8$, and 1.0 (from *top* to *bottom*). The numerical results approach the predicted geometrical optics limits [16, 21] $\sigma_{\text{abs}}/M^2 \simeq 21.21, 19.38, 16.23$, and 12.57, respectively, which are indicated by *straight lines*. In these numerical experiments, we have set $N_{\text{max}} = 400$ and maximum map parameter $L_0 = 30$

where $x_\pm$ indicates the positions of the horizons of the black hole for the case $q < 1$. For the extremal case, there is only one horizon ($x = 1/2$).

The boundary conditions are the same as in Eq. (3), and the application of the spectral algorithm is straightforward. We have solved the scattering problem for $q = 0.5, 0.8$ and $q = 1.0$. The results are summarized in Fig. 9 with the total absorption cross sections for these values of the charge. Notice that the increase of charge produces a decrease of the total absorption cross section [21]. Also, we have obtained the correct geometrical optics limits predicted analytically [16].

4.2 Electromagnetic and Gravitational Perturbations

We follow the notation of Chandrasekhar and represent $H_1^{(\pm)}(x_*)$ and $H_2^{(\pm)}(x_*)$, which are the electromagnetic and gravitational perturbations, respectively. Their corresponding equations of motion can be decoupled [4, 22] with the introduction of two functions, $Z_1^{(\pm)}(x_*)$, $Z_2^{(\pm)}(x_*)$, that satisfy a Schrodinger-like equation (2). The signs $\pm$ indicate that the perturbations consist of polar (even parity) or axial (odd parity) modes, respectively. The relevant equations can be summarized as [4, 22]

$$\frac{d^2 Z_i^{(\pm)}}{dx_*^2} + \left(\omega^2 - V_i^{(\pm)}\right) Z_i^{(\pm)} = 0, \tag{35}$$

where $i = 1, 2$ and the effective potentials are given by

$$V_i^{(-)} = f(x)\left[\frac{l(l+1)}{x^2} - \frac{q_j}{2x^3}\left(1 + \frac{q_i}{2\mu^2 x}\right)\right]$$

$$V_i^{(+)} = V_i^{(-)} + 2q_j f(x)\frac{d}{dx}\left[\frac{f(x)}{x(2\mu^2 x + q_j)}\right]. \tag{36}$$

In the above expressions, $i \neq j$, $q = Q/M$, $\mu^2 = (l-1)(l+2)$, and

$$q_1 = 3 + \sqrt{9 + 4q^2\mu^2}, \quad q_2 = 3 - \sqrt{9 + 4q^2\mu^2}. \tag{37}$$

We are interested in the solutions of Eq. (35) satisfying the following asymptotic behavior:

$$Z_i^{(\pm)} = \begin{cases} e^{-i\omega x_*} + \alpha_i^{(\pm)} e^{i\omega x_*} & x_* \to \infty \\ \beta_i^{(\pm)} e^{-i\omega x_*}, & x_* \to -\infty. \end{cases} \tag{38}$$

As before, since the effective potentials $V_i^{(\pm)}$ are real, the following conservation law holds:

$$R_i(\omega) + T_i(\omega) = 1, \tag{39}$$

where $i = 1, 2$, $R_i(\omega) = |\alpha_i^{(\pm)}|^2$, and $T_i(\omega) = |\beta_i^{(\pm)}|^2$.

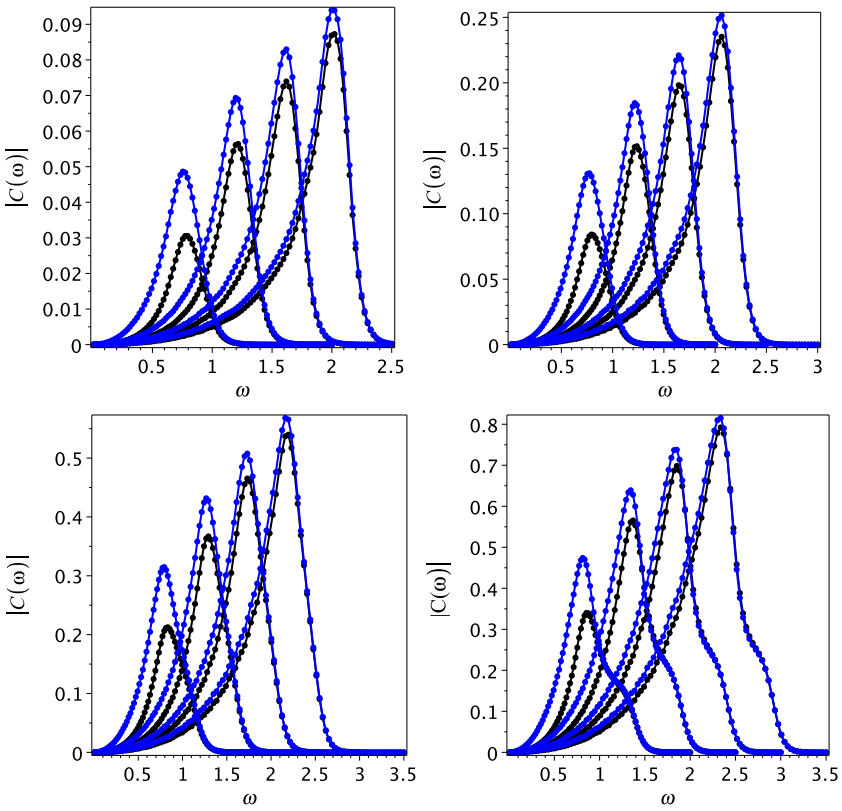

Fig. 10 (Colored online) Plots of the conversion factor (Eq. (40)) for $q = 0.3, 0.5, 0.8, 0.99$ (from *left* to *right*, *up* and *down*). The results for axial perturbations are in *black* while those for polar perturbations are in *blue*. In all figures, we read $l = 2, 3, 4, 5$ from *left* to *right*. In all cases, $L_0 = 50$ and $N = 600$

We have applied the spectral algorithm to solve the scattering problem governed by Eq. (35) with boundary condition (38), to determine the complex coefficients $\alpha_i^{(\pm)}(\omega)$, $\beta_i^{(\pm)}(\omega)$ for several values of q and l. The accuracy of the solutions was monitored by the conservation law (39), not allowing $\delta = |R_i(\omega) + T_i(\omega) - 1| \times 100$ to be greater than 0.2 %.

The most interesting phenomenon in the present case is the conversion of gravitational to electromagnetic perturbations, and vice-versa. The conversion factor from an incident perturbation which is entirely from one form (electromagnetic or gravitational) that is reflected of the other is given by [4, 23, 24]

$$|\mathcal{C}^{(\pm)}(\omega)| = \frac{1}{4}|\alpha_1^{(\pm)}(\omega) - \alpha_2^{(\pm)}(\omega)|^2 \sin^2(2\psi), \tag{40}$$

where [4, 22]

$$\sin^2(2\psi) = \mp 2q\sqrt{\frac{(l-1)(l+2)}{9+4q^2(l-1)(l+2)}}. \tag{41}$$

Another equivalent expression for the conversion factor, $|\mathcal{C}^{(\pm)}(\omega)| = \left(R_1 + R_2 - 2\sqrt{R_1 R_2}\cos\left(\delta_1^{(\pm)} - \delta_2^{(\pm)}\right)\right)\sin^2(2\psi)/4$, is obtained if we consider $\alpha_j^{(\pm)}(\omega) = \sqrt{R_j(\omega)}\exp(i\delta_j^{(\pm)})$, $j = 1, 2$, where $\delta_j^{(\pm)}$ are the phases of reflected waves. Although the reflection coefficients do not depend on the parity, this is no longer valid for the reflected phases. Therefore, the conversion factor $|\mathcal{C}^{(\pm)}(\omega)|$ represents one of the few aspects of the black hole physics in which the parity has a direct influence.

After solving the scattering problem for both effective potentials, we have focused on determining the conversion factor $|\mathcal{C}^{(\pm)}(\omega)|$. In Fig. 10, we show the conversion factor for $q = 0.3, 0.5, 0.8, 0.99$ and taking $l = 2, ..., 5$. Note that the conversion factors for polar perturbations are larger than those corresponding to axial perturbations, which is also confirmed by Gunter [23] and Crispino et al. [25].

5 Conclusions

In this work, we have adapted Boyd's spectral algorithm [1] to solve the black hole scattering problem. One of the main achievements of Boyd's algorithm was the introduction of the radiative functions, allowing to overcome the limitation of the basis functions to model the incoming and outgoing waves due to the rapid oscillatory behavior at the boundaries. Boyd has used the standard rational Chebyshev polynomials as the basis functions, but here we have considered a new set of basis functions obtained by a suitable combination of these polynomials. As a consequence, a considerable gain in the accuracy was obtained. Another modification was the introduction of the parameter ϵ_0 assumed to be proportional to the inverse of L_0.

We successfully have applied the spectral code to solve the scattering problem for the Schwarzschild, canonical acoustic, and Reissner–Nordström black holes. These problems exhibited a considerable degree of difficulty not found in the example treated by Boyd, which consisted in a symmetric sech^2 potential barrier. As pointed out by Boyd [1], very high accuracy is required to determine the tiny reflection coefficient for high frequencies. We have used $N = 600$ as the maximum truncation order, but the appropriate choice of the map parameter L_0 was a very important factor for the accuracy of the results. We have considered scalar ($s = 0$), electromagnetic ($s = 1$), and gravitational ($s = 2$) perturbations for the cases of Schwarzshild and Reissner–Nordström black holes, but the case of neutrino ($s = 1/2$) waves could be well considered. In general, the results are in agreement with the corresponding of previous studies on black hole scattering. We have determined precisely the exponential decay of the small reflection coefficient in each case of interest. According to the numerical experiments, κ tends to a limit value for large l in all cases.

We intend to study the wave scattering by a Kerr black hole due its astrophysical relevance. In this case, the code needs to be modified due to the slight variation of the boundary conditions [26, 27]. Also, another wave scattering problem of interest is due to a black hole in AdS spacetime, where the motivation arises from the AdS/CFT conjecture. In this case, the code needs to be further modified in view of the spacetime not being asymptotically flat.

Acknowledgments The authors thank John Boyd for the fruitful discussions about his spectral algorithm for the scattering problem and Luís C.B. Crispino for the several discussions and valuable references. We also thank the following Brazilian scientific agencies for the financial support: Conselho Nacional de Desenvolvimento Científico e Tecnológico, CNPq; Coordenação de Aperfeiçoamento de Pessoal de Nível Superior, CAPES; and Fundação de Amparo a Pesquisa do Estado do Rio de Janeiro, FAPERJ.

References

1. J.P. Boyd, Comp. Phys. **4**, 83 (1990)
2. R.A. Matzner, Phys. J. Math. **9**, 163 (1968)
3. J.A.H. Futterman, F.A. Handler, R.A. Matzner, *Scattering from Black Holes* (Cambridge University Press, Cambridge, 1988)
4. S. Chandrasekhar, *The Mathematical Theory of Black Holes* (Oxford University Press, 1983)
5. T. Regge, J.A. Wheeler, Phys. Rev. **108**, 1063 (1957)
6. K.D. Kokotas, B.G. Schmidt, Quasi-normal modes of stars and black holes. Living Rev. Relativ. **2**, 2 (1999)
7. N. Sanchez, Black Holes: Scatterers, Absorbers and Emitters of Particles (2001). arXiv:hep-th/0106222
8. N. Andersson, Phys. Rev. D **52**, 1808 (1995)
9. J.P. Boyd. *Weakly Nonlocal Solitary Waves and Beyond-All-Orders Asymptotics* (Kluwer, Boston, 1998)

10. J.P. Boyd. *Chebyshev and Fourier Spectral Methods* (Dover, New York, 2001)
11. W. Heinrichs, J. Comp. Phys. **59**, 103 (1989)
12. W. Heinrichs, J. Scient. Comp. **6**, 1 (1991)
13. W. Heinrichs, SIAM J. Scient. Stat. Comp. **12**, 1162 (1991)
14. F.J. Zerilli, Phys. Rev. D **2**, 2141 (1970)
15. K. Gottfried, T.M. Yan. *Quantum Mechanics: Fundamentals,* 2nd edn. (Springer, New York, 2004)
16. B. Mashhoon, Phys. Rev. D **7**, 2807 (1973)
17. M. Visser, Class. Quantum Grav. **15**, 1767 (1998)
18. S. Weinfurtner, E.W. Tedford, M.C.J. Penrice, W.G. Unruh1, G.A. Lawrence, Phys. Rev. Lett. **106**, 21302 (2011)
19. S.R. Dolan, E.S. Oliveira, L.C.B. Crispino, Phys. Rev. D **64014**, 79 (2009)
20. S. Chandrasekhar, Proc. R. Soc. Lond. A **365**, 453 (1979)
21. L.C.B. Crispino, S. Dolan, E.S. Oliveira, Phys. Rev. D **79**, 64022 (2009)
22. V. Moncrief, Phys. Rev. D. **9**, 2707 (1974)
23. D.L. Gunter, Phil. Trans. R. Soc. Lond. A **299**, 497 (1980)
24. D.W. Olson, W.G. Unruh, Phys. Rev. Lett. **33**, 1116 (1974)
25. L.C.B. Crispino, A. Higuchi, E.S. Oliveira, Phys. Rev. D **80**, 104026 (2009)
26. K. Glampedakis, N. Andersson, Class. Quant. Grav. **18**, 1939 (2001)
27. C.F.B. Macedo, L.C.B. Crispino, V. Cardoso, Phys. Rev. D **86**, 24002 (2012)